Supporting Information:

Computation of Solid-State Vibrational Circular Dichroism in the Periodic Gauge

Sascha Jähnigen,[*,†,‡] Anne Zehnacker,[†] and Rodolphe Vuilleumier[*,‡]

†*Institut des Sciences Moléculaires d'Orsay (ISMO), CNRS, Université Paris-Saclay,*
91405 Orsay, France

‡*PASTEUR, Département de Chimie, Ecole Normale Supérieure, PSL University,*
Sorbonne Université, CNRS, 75005 Paris, France

E-mail: sascha.jahnigen@ens.psl.eu; rodolphe.vuilleumier@ens.psl.eu

Rotational Strength for Periodic Boundaries

In this section, we discuss the gauge dependence of the classical time-correlation function of the electric current and magnetic dipole moment for periodic boundary conditions (PBC) and propose a gauge-independent expression of the resulting VCD signal.

Position of the Problem

We consider the calculation of a susceptibility of the following type:

$$\chi_{jm}(\omega) = \int_{-\infty}^{\infty} \langle \mathbf{j}(0) \cdot \mathbf{m}(t) \rangle \, e^{i\omega t} dt, \tag{1}$$

where $\mathbf{j}(t)$ is the time-derivative of the system's instantaneous electric dipole moment (current dipole moment), and $\mathbf{m}(t)$ its instantaneous magnetic dipole moment. We assume that both

observables can be decomposed as sum of local contributions:

$$\mathbf{j}(t) = \sum_i \mathbf{j}_i(t) \tag{2}$$

and

$$\mathbf{m}(t) = \sum_i \mathbf{m}_i(t). \tag{3}$$

For the electronic wave function this is done through localisation of the orbitals, usually *maximally localised Wannier functions* (MLWF)[S1] i can label a whole molecule if the localised orbitals are assigned to molecules (this work), or run over nuclei, MLWFs, as well as atoms in a force field approach. For each subsystem, or fragment, i an individual, local, gauge has been defined such that the magnetic moment and that it can be written as the sum of a local gauge (LG) contribution and gauge transport (GT) contribution:

$$\mathbf{m}_i(t) = \mathbf{m}_{i,\mathrm{LG}}(t) + \mathbf{m}_{i,\mathrm{GT}}^{\mathcal{O}}(t), \tag{4}$$

where the gauge transport term with respect to a common origin $\mathcal{O}$ can be written as

$$\mathbf{m}_{i,\mathrm{GT}}^{\mathcal{O}}(t) = \frac{1}{2c}\overrightarrow{\mathcal{O}\mathbf{r}_i} \times \mathbf{j}_i \tag{5}$$

where $\mathbf{r}_i$ is the fragment-dependent local origin of the local gauge (e.g., centre of mass of a molecule). This poses a twofold problem:

(I) If an other choice of origin $\mathcal{O}'$ is chosen then each fragment magnetic moment transforms as

$$\mathbf{m}_i^{\mathcal{O}'} = \mathbf{m}_i^{\mathcal{O}} + \frac{1}{2c}\overrightarrow{\mathcal{O}'\mathcal{O}} \times \mathbf{j}_i(t) \tag{6}$$

and the overall magnetic moment transforms as

$$\mathbf{m}^{\mathcal{O}'} = \mathbf{m}^{\mathcal{O}} + \frac{1}{2c}\overrightarrow{\mathcal{O}'\mathcal{O}} \times \mathbf{j}(t). \tag{7}$$

The GT term thus renders the whole magnetic moment gauge-dependent.

(II) The vector position of fragment i, $\overrightarrow{\mathcal{O}\mathbf{r}_i}$, with respect to a global origin $\mathcal{O}$ is ill-defined in PBC.

We will first examine how the overall VCD signal, i.e., the susceptibility $\chi_{jm}(\omega)$, can be gauge independent while the magnetic moment is not. Then we will derive an alternative expression that is explicitly gauge independent. This will have two advantages: We can expect to limit the noise on $\chi_{jm}(\omega)$ from the GT term since we do no longer rely on the cancellation of opposite sign terms. The main advantage, however, will be that this expression will be properly defined for PBC.

Gauge Independence of the Susceptibility

General idea

Briefly, the main point of the derivation is that the susceptibility $\chi_{jm}(\omega)$ transforms following a change of origin from $\mathcal{O}$ to $\mathcal{O}'$ as

$$\chi_{jm}^{\mathcal{O}'}(\omega) = \chi_{jm}^{\mathcal{O}}(\omega) + \frac{1}{2c}\overrightarrow{\mathcal{O}'\mathcal{O}} \times \chi_{jj}(\omega). \tag{8}$$

However, the current-current susceptibility $\chi_{jj}(\omega)$ is a symmetric tensor such that the gauge transport term in the previous expression is zero because of the cross-product.

T-Symmetry of the Correlation Function

In the Heisenberg representation the rotational strength is defined by means of the quantum time-correlation function, yet the latter can be transformed, as described by Kubo,[S2] to relate to the classical time-correlation function. Taking the classical limit, a quantum correction factor can be added *a posteriori*.[S3]

We consider the classical time-correlation function (TCF), but the results remains true in the quantum case if Kubo transformed correlation functions are used instead of the original quantum correlation function.

Considering that all observables A considered here, $\mathbf{m}$ or $\mathbf{j}$, transform by time reversal as $A \to -A$, we easily find

$$\langle A(0)B(t)\rangle = \langle A(0)B(-t)\rangle = \langle A(t)B(0)\rangle = \langle B(0)A(t)\rangle. \tag{9}$$

The second equality relies on the stationarity of the TCF and is exact only in the limit of an infinite trajectory.

Proof of the Gauge Independence of the Susceptibility

Using Einstein's notation (repeated indices indicate a sum over x, y, z), from T-symmetry it follows that the current-current susceptibility is symmetric:

$$
\begin{aligned}
\chi_{jj,\alpha\beta}(\omega) &= \int_{-\infty}^{\infty} \langle j_\alpha(0)j_\beta(t)\rangle \, e^{i\omega t} dt \\
&= \int_{-\infty}^{\infty} \langle j_\beta(0)j_\alpha(t)\rangle \, e^{i\omega t} dt \\
&= \chi_{jj,\beta\alpha}(\omega).
\end{aligned}
\tag{10}
$$

Then from

$$\chi_{jm,\alpha\alpha}^{\mathcal{O}'}(\omega) = \chi_{jm,\alpha\alpha}^{\mathcal{O}}(\omega) + \frac{1}{2c}\epsilon_{\alpha\beta\gamma} \cdot (\mathcal{O}'\mathcal{O})_\beta \cdot \chi_{jj,\alpha\gamma}(\omega), \tag{11}$$

where $\epsilon_{\alpha\beta\gamma}$ is the Levi-Civita tensor satisfying $\epsilon_{\alpha\beta\gamma} = -\epsilon_{\gamma\beta\alpha} = -\epsilon_{\alpha\gamma\beta}$, we can verify that

$$
\begin{aligned}
\epsilon_{\alpha\beta\gamma} \cdot (\mathcal{O}'\mathcal{O})_\beta \cdot \chi_{jj,\alpha\gamma}(\omega) &= \epsilon_{\gamma\beta\alpha} \cdot (\mathcal{O}'\mathcal{O})_\beta \cdot \chi_{jj,\gamma\alpha}(\omega) \\
&= -\epsilon_{\alpha\beta\gamma} \cdot (\mathcal{O}'\mathcal{O})_\beta \cdot \chi_{jj,\gamma\alpha}(\omega) \\
&= 0,
\end{aligned}
\tag{12}
$$

Gauge invariance is then readily obtained.

Expression of the Susceptibility that is Explicitly Origin-Independent

From the decomposition of the current and magnetic dipole moments into fragment contributions, we have, using Einstein's notation:

$$\chi^{\mathcal{O}}_{jm,\alpha\alpha}(\omega) = \int_{-\infty}^{\infty} \sum_{ij} \left[\langle j_{i,\alpha}(0) m_{j,\text{LG},\alpha}(t) \rangle + \frac{1}{2c} \langle j_{i,\alpha}(0) \left(\epsilon_{\alpha\beta\gamma} (\mathcal{O}r_j(t))_\beta \cdot j_{j,\gamma}(t) \right) \rangle \right] e^{i\omega t} dt$$

$$= \int_{-\infty}^{\infty} \sum_{ij} \left[\langle j_{i,\alpha}(0) m_{j,\text{LG},\alpha}(t) \rangle + \frac{1}{2c} \epsilon_{\alpha\beta\gamma} \langle j_{i,\alpha}(0) \left((\mathcal{O}r_j(t))_\beta \cdot j_{j,\gamma}(t) \right) \rangle \right] e^{i\omega t} dt$$

(13)

(NB: the subscript LG has been dropped in the main text). It is important to remember that the Einstein sum is taken over repeated indices and that their symbols can be interchanged. With T-symmetry of the correlation function it follows:

$$\chi^{\mathcal{O}}_{jm,\alpha\alpha}(\omega) = \int_{-\infty}^{\infty} \sum_{ij} \left[\langle j_{i,\alpha}(0) m_{j,\text{LG},\alpha}(t) \rangle + \frac{1}{2c} \epsilon_{\alpha\beta\gamma} \langle j_{i,\alpha}(0) \left((\mathcal{O}r_j(t))_\beta \cdot j_{j,\gamma}(t) \right) \rangle \right] e^{i\omega t} dt$$

$$= \int_{-\infty}^{\infty} \sum_{ij} \left[\langle j_{i,\alpha}(0) m_{j,\text{LG},\alpha}(t) \rangle - \frac{1}{2c} \epsilon_{\beta\alpha\gamma} \langle j_{i,\alpha}(0) \left((\mathcal{O}r_j(t))_\beta \cdot j_{j,\gamma}(t) \right) \rangle \right] e^{i\omega t} dt$$

$$= \int_{-\infty}^{\infty} \sum_{ij} \left[\langle j_{i,\alpha}(0) m_{j,\text{LG},\alpha}(t) \rangle - \frac{1}{2c} \epsilon_{\beta\alpha\gamma} \langle \left((\mathcal{O}r_j(0))_\beta \cdot j_{j,\gamma}(0) \right) j_{i,\alpha}(t) \rangle \right] e^{i\omega t} dt \quad (14)$$

$$= \int_{-\infty}^{\infty} \sum_{ij} \left[\langle j_{i,\alpha}(0) m_{j,\text{LG},\alpha}(t) \rangle - \frac{1}{2c} \epsilon_{\beta\gamma\alpha} \langle \left((\mathcal{O}r_j(0))_\beta \cdot j_{j,\alpha}(0) \right) j_{i,\gamma}(t) \rangle \right] e^{i\omega t} dt$$

$$= \int_{-\infty}^{\infty} \sum_{ij} \left[\langle j_{i,\alpha}(0) m_{j,\text{LG},\alpha}(t) \rangle - \frac{1}{2c} \epsilon_{\alpha\beta\gamma} \langle j_{i,\alpha}(0) \left((\mathcal{O}r_i(0))_\beta \cdot j_{j,\gamma}(t) \right) \rangle \right] e^{i\omega t} dt,$$

where in the last line, after cyclic shift of the triple product, the indices i and j have been exchanged as they are summed over as well. It is now easy to take the half of the sum of the first and last line to obtain

$$\chi^{\mathcal{O}}_{jm,\alpha\alpha}(\omega) = \int_{-\infty}^{\infty} \sum_{ij} \left[\langle j_{i,\alpha}(0) m_{j,\text{LG},\alpha}(t) \rangle + \frac{1}{4c} \epsilon_{\alpha\beta\gamma} \langle j_{i,\alpha}(0) \left(\mathcal{O}r_j(t) - \mathcal{O}r_i(0) \right)_\beta \cdot j_{j,\gamma}(t) \rangle \right] e^{i\omega t} dt$$

$$= \int_{-\infty}^{\infty} \sum_{ij} \left[\langle j_{i,\alpha}(0) m_{j,\text{LG},\alpha}(t) \rangle + \frac{1}{4c} \epsilon_{\alpha\beta\gamma} \langle j_{i,\alpha}(0) \left(r_i(0) r_j(t) \right)_\beta \cdot j_{j,\gamma}(t) \rangle \right] e^{i\omega t} dt.$$

(15)

The last expression is explicitly gauge independent as the origin $\mathcal{O}$ has completely disappeared and only the vector $(\mathbf{r}_j(t) - \mathbf{r}_i(0))$ is involved. After dropping the superscript $\mathcal{O}$ the susceptibility reads:

$$\chi_{jm,\alpha\alpha}(\omega) = \int_{-\infty}^{\infty} \sum_{ij} \left[\langle j_{i,\alpha}(0) m_{j,\mathrm{LG},\alpha}(t) \rangle + \frac{1}{4c} \epsilon_{\alpha\beta\gamma} \langle j_{i,\alpha}(0) \left(r_i(0) r_j(t) \right)_\beta \cdot j_{j,\gamma}(t) \rangle \right] e^{i\omega t} dt. \quad (16)$$

It should be noted that the self-term $i = j$ does not cancel. This can be understood, for instance, as a fragment moving along a helix.

Minimum Image Convention

The minimum image convention ensures that pair distances are always between adjacent (nearest) neighbours taking the periodic image if necessary. This convention can be expressed through lattice translation $\Delta_{ij}^{\mathrm{PBC}}$ (see main text), adding integer units $(a = -1, 0, 1)$ of the lattice vector for each axis,

$$\overrightarrow{\mathbf{r}_i \mathbf{r}_j} = \mathbf{r}_j - \mathbf{r}_i + \Delta_{ij}^{\mathrm{PBC}}. \quad (17)$$

Considering the minimum-image convention through $\Delta_{ij}^{\mathrm{PBC}}$ and using the correlation time τ, the GT term can be transformed, so that the distributed origins $\mathbf{r}_i$ enter individually (with respect to the common origin) and that only $\Delta_{ij}^{\mathrm{PBC}}$ depends on i and j. Using the

T-symmetry of the correlation function, it follows:

$$
\epsilon_{\alpha\beta\gamma} \left\langle j_{i,\alpha}(t)\, (r_i(t)r_j(t+\tau))_\beta \cdot j_{j,\gamma}(t+\tau) \right\rangle
$$

$$
= \epsilon_{\alpha\beta\gamma} \left\langle j_{i,\alpha}(t)\, \left(r_j(t+\tau) - r_i(t) + \Delta_{ij}^{\mathrm{PBC}}(t,t+\tau)\right)_\beta \cdot j_{j,\gamma}(t+\tau) \right\rangle
$$

$$
= \epsilon_{\alpha\beta\gamma} \left\langle j_{i,\alpha}(t) r_j(t+\tau)_\beta \cdot j_{j,\gamma}(t+\tau) \right\rangle
$$

$$
\quad - \epsilon_{\alpha\beta\gamma} \left\langle j_{i,\alpha}(t) r_i(t)_\beta \cdot j_{j,\gamma}(t+\tau) \right\rangle \;+\; \epsilon_{\alpha\beta\gamma} \left\langle j_{i,\alpha}(t) \Delta_{ij}^{\mathrm{PBC}}(t,t+\tau)_\beta \cdot j_{j,\gamma}(t+\tau) \right\rangle
$$

$$
= \epsilon_{\alpha\beta\gamma} \left\langle j_{i,\alpha}(t) r_j(t+\tau)_\beta \cdot j_{j,\gamma}(t+\tau) \right\rangle
$$

$$
\quad - \epsilon_{\gamma\alpha\beta} \left\langle j_{j,\gamma}(t+\tau) j_{i,\alpha}(t) \cdot r_i(t)_\beta \right\rangle \;+\; \epsilon_{\alpha\beta\gamma} \left\langle j_{i,\alpha}(t) \Delta_{ij}^{\mathrm{PBC}}(t,t+\tau)_\beta \cdot j_{j,\gamma}(t+\tau) \right\rangle
$$

$$
= \epsilon_{\alpha\beta\gamma} \left\langle j_{i,\alpha}(t) r_j(t+\tau)_\beta \cdot j_{j,\gamma}(t+\tau) \right\rangle \tag{18}
$$

$$
\quad + \epsilon_{\gamma\beta\alpha} \left\langle j_{j,\gamma}(t+\tau) r_i(t)_\beta \cdot j_{i,\alpha}(t) \right\rangle \;+\; \epsilon_{\alpha\beta\gamma} \left\langle j_{i,\alpha}(t) \Delta_{ij}^{\mathrm{PBC}}(t,t+\tau)_\beta \cdot j_{j,\gamma}(t+\tau) \right\rangle
$$

$$
= \epsilon_{\alpha\beta\gamma} \left\langle j_{i,\alpha}(t) r_j(t+\tau)_\beta \cdot j_{j,\gamma}(t+\tau) \right\rangle
$$

$$
\quad + \epsilon_{\gamma\beta\alpha} \left\langle j_{i,\gamma}(t) r_j(t+\tau)_\beta \cdot j_{j,\alpha}(t+\tau) \right\rangle \;+\; \epsilon_{\alpha\beta\gamma} \left\langle j_{i,\alpha}(t) \Delta_{ij}^{\mathrm{PBC}}(t,t+\tau)_\beta \cdot j_{j,\gamma}(t+\tau) \right\rangle
$$

$$
= \epsilon_{\alpha\beta\gamma} \left\langle j_{i,\alpha}(t) r_j(t+\tau)_\beta \cdot j_{j,\gamma}(t+\tau) \right\rangle
$$

$$
\quad + \epsilon_{\alpha\beta\gamma} \left\langle j_{i,\alpha}(t) r_j(t+\tau)_\beta \cdot j_{j,\gamma}(t+\tau) \right\rangle \;+\; \epsilon_{\alpha\beta\gamma} \left\langle j_{i,\alpha}(t) \Delta_{ij}^{\mathrm{PBC}}(t,t+\tau)_\beta \cdot j_{j,\gamma}(t+\tau) \right\rangle
$$

$$
= 2 \cdot \epsilon_{\alpha\beta\gamma} \left\langle j_{i,\alpha}(t) r_j(t+\tau)_\beta \cdot j_{j,\gamma}(t+\tau) \right\rangle \;+\; \epsilon_{\alpha\beta\gamma} \left\langle j_{i,\alpha}(t) \Delta_{ij}^{\mathrm{PBC}}(t,t+\tau)_\beta \cdot j_{j,\gamma}(t+\tau) \right\rangle
$$

$$
\approx 2 \cdot \epsilon_{\alpha\beta\gamma} \left\langle j_{i,\alpha}(t) r_j(t+\tau)_\beta \cdot j_{j,\gamma}(t+\tau) \right\rangle \;+\; \epsilon_{\alpha\beta\gamma} \left\langle j_{i,\alpha}(t) \Delta_{ij}^{\mathrm{PBC}}(t)_\beta \cdot j_{j,\gamma}(t+\tau) \right\rangle
$$

The latter approximation allows for using FFT for the computation of the TCF, which would otherwise be computationally very demanding for $\Delta_{ij}^{\mathrm{PBC}}(t+\tau)$ would have to be evaluated for each pair $(t, t+\tau)$. As a consequence, if a particle diffuses too fast within correlation time τ, there may occur jumps in the TCF. For the term $\mathbf{r}_j(t) \times \mathbf{j}_j(t)$, this can be circumvented by unwrapping the periodic boundaries *a priori*. In turn, for $\Delta_{ij}^{\mathrm{PBC}}(t, t+\tau) \times \mathbf{j}_j(t, t+\tau)$ there is no such operation. However, the approximation made in the last line of the upper equation can be connected to a condition. If $\Delta_{ij}^{\mathrm{PBC}}(t)$ shall be used, the inequality $r_{\alpha,j}(t+\tau) - r_{\alpha,i}(t) \leq \frac{1}{2}|T_\alpha|$ has to be satisfied, where $\mathbf{T}$ is the cell tensor. Hence, for large cells (liquids) and/or slow relative particle diffusion (solids), the approximation $\Delta_{ij}^{\mathrm{PBC}}(t, t+\tau) \approx \Delta_{ij}^{\mathrm{PBC}}(t)$ is valid.

Periodic case

The resulting expression for the susceptibility reads:

$$\chi_{jm,\alpha\alpha}(\omega) = \int_{-\infty}^{\infty} \sum_{ij} \left[\left\langle j_{i,\alpha}(0)m_{j,\text{LG},\alpha}(t) \right\rangle \right.$$
$$\left. + \frac{1}{2c}\epsilon_{\alpha\beta\gamma} \left\langle j_{i,\alpha}(0)\left(r_j(t) + \frac{1}{2}\Delta_{ij}^{\text{PBC}}(0)\right)_\beta \cdot j_{j,\gamma}(t) \right\rangle \right] e^{i\omega t} dt. \tag{19}$$

The sum over j can be carried out *a priori*, which scales the algorithm from $O(N_i \cdot N_j) = O(N_i^2)$ to $O(N_i)$. The final expression is:

$$\chi_{jm,\alpha\alpha}(\omega) = \int_{-\infty}^{\infty} \left[\left\langle j_\alpha(0)m_{\text{LG},\alpha}(t) \right\rangle \right.$$
$$\left. + \frac{1}{2c}\epsilon_{\alpha\beta\gamma} \sum_i \left\langle j_{i,\alpha}(0) \sum_j \left(r_j(t) + \frac{1}{2}\Delta_{ij}^{\text{PBC}}(0)\right)_\beta \cdot j_{j,\gamma}(t) \right\rangle \right] e^{i\omega t} dt. \tag{20}$$

Isolated case

For the non-periodic case this simplifies to a single calculation:

$$\chi_{jm,\alpha\alpha}(\omega) = \int_{-\infty}^{\infty} \left[\left\langle j_\alpha(0)m_{\text{LG},\alpha}(t) \right\rangle + \frac{1}{2c}\epsilon_{\alpha\beta\gamma} \left\langle j_\alpha(0) \sum_j r_j(t)_\beta \cdot j_{j,\gamma}(t) \right\rangle \right] e^{i\omega t} dt. \tag{21}$$

Pseudo-isolated case

This relation holds under pseudo-isolated conditions (*e.g.*, a solute in a solvent bath), with a distance cutoff r_c applied around an origin molecule $\mathbf{r}_k$, if $\mathbf{r}_j$ is defined relative to the origin, $\mathbf{r}_j^k(t) = \mathbf{r}_j(t) + \Delta_{kj}^{\text{PBC}}(t)$, and $r_c \leq \frac{1}{4}|T_\alpha|$, where $\mathbf{T}$ is the cell tensor:

$$\chi_{jm,\alpha\alpha}(\omega) = \int_{-\infty}^{\infty} \left[\left\langle j_\alpha(0)m_{\text{LG},\alpha}(t) \right\rangle + \frac{1}{2c}\epsilon_{\alpha\beta\gamma} \left\langle j_\alpha(0) \sum_j r_j^k(t)_\beta \cdot j_{j,\gamma}(t) \right\rangle \right] e^{i\omega t} dt \tag{22}$$

This almost, but not exactly, equals the entry expression for $\chi^{\mathcal{O}}_{jm,\alpha\alpha}(\omega)$, where it has been assumed $\overrightarrow{\mathcal{O}\mathbf{r}_j}(t) = \mathbf{r}_j(t) - \mathcal{O} + \Delta^{\text{PBC}}_{\mathcal{O}j}(t)$
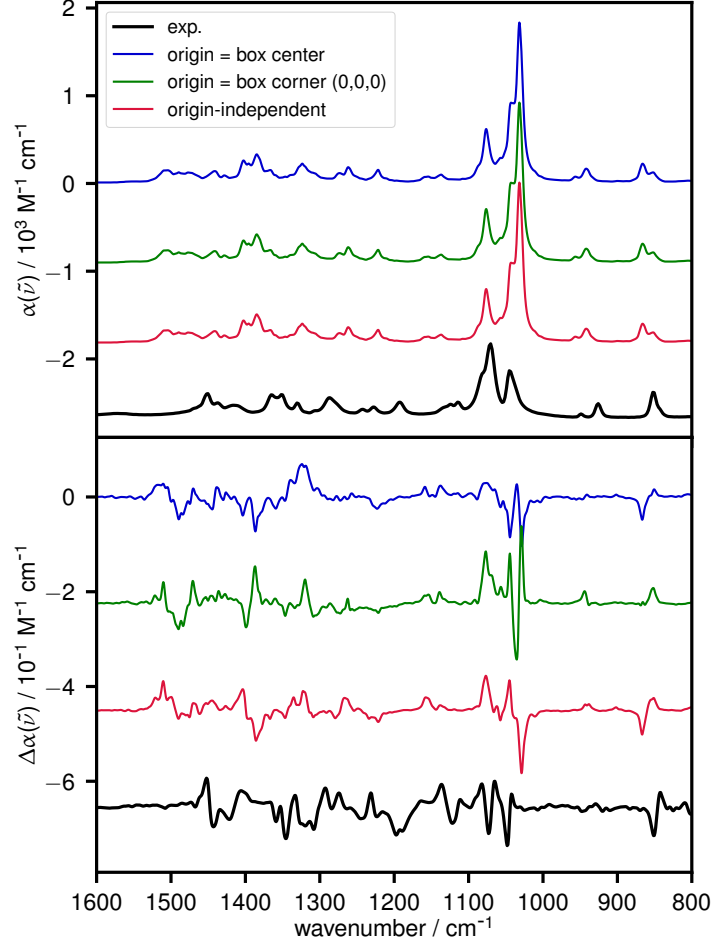

Figure S1: Gauge dependence of the VCD spectrum using the old (Equation 8 in the main text), and the new (Equation 9 in the main text) formulation of the rotational strength. For this figure, no frequency alignment has been carried out.

Experimental Methods
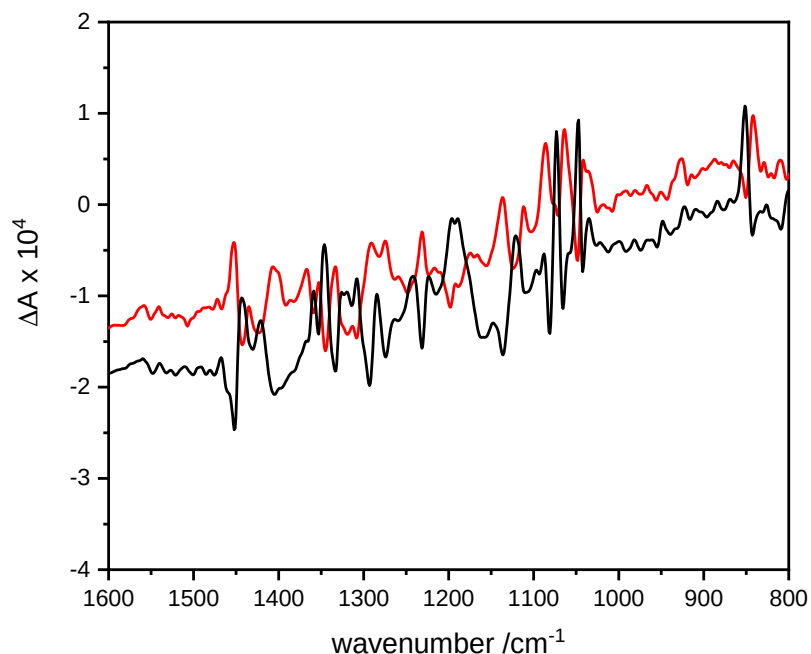
Figure S2: The mid-IR VCD spectra of solid-state (1R,2R)-*trans*-1,2-cyclohexanediol (black) and (1S,2S)-*trans*-1,2-cyclohexanediol (red) in a KBr pellet, at a mass concentration of 0.5%.

The IR absorption and VCD spectra of the enantiopure forms of solid (1S,2S)-*trans*-1,2-cyclohexanediol were measured using a Fourier-transform infrared spectroscopy (FTIR) spectrometer (Vertex 70, Bruker) equipped with a VCD module (PMA 50, Bruker), as previously described.[S4–S7] The filtered and linearly polarized IR radiation was modulated by a 50 kHz ZnSe photo-elastic modulator (Hinds). The signal was measured by a mercury-cadmium-telluride (MCT) IR detector and demodulated by a lock-in amplifier (Stanford Research Systems SR 830), with a spectral resolution of 4 cm^{-1}. The samples were prepared by grinding 10 mg of enantiopure (1S,2S)-*trans*-1,2-cyclohexanediol with 2 g of KBr in a mixer mill (MM 400 Retsch) at 20 Hz during 30 min and making 150 to 200 mg pellets in an hydraulic press. Linear dichroism artefacts were eliminated following the procedure reported in the literature.[S8,S9] It consists in averaging the spectra obtained for the pellets

rotated at 0° and 90° in the plane perpendicular to the light propagation axis for each side of the pellet. Each measurement corresponds to a total measurement time of 4 h and was repeated on two different pellets to ensure its reproducibility. When not specified otherwise, the VCD spectrum discussed in the article is that of $(1S,2S)$-*trans*-1,2-cyclohexanediol obtained from the half difference of the VCD spectra of the two enantiomers, shown in Figure S2. $(1R,2R)$-*trans*-1,2-cyclohexanediol and $(1S,2S)$-*trans*-1,2-cyclohexanediol were purchased from Sigma-Aldrich and used without further purification.

Computational Details

Molecular Dynamics, Quantum Response, Gauge and Correlation

A single unit cell of crystalline (1S,2S)-*trans*-1,2-cyclohexanediol was considered based on the crystal structure from diffraction taken from the CCDC database (CCDC 974135).[S10] (1S,2S)-*trans*-1,2-cyclohexanediol crystallises in the $P3_121$ space group with cell parameters $a = b = 10.216$ Å, $c = 10.884$ Å, $\alpha = \beta = 90.00°$, $\gamma = 120.00°$. The system was optimised an pre-equilibrated using CP2K 6.1[S11] and AmberTools20[S12] with the GAFF2 force field.[S12] Then, Born-Oppenheimer AIMD simulations were carried out with the CP2K 5.1[S11] program package via the Quickstep module,[S13] describing the exchange-correlation energy with the GGA functional BLYP for equilibration and the hybrid functional B3LYP for production (30 ps),[S14–S18] the DZVP-MOLOPT-SR-GTH basis set,[S19] and GTH pseudo-potentials[S20–S22] with a 0.5 fs time step, a density cutoff of 400 Ry, and Grimme's dispersion correction (D3).[S23] The CSVR[S24] thermostat was used at 320 K to account for the overstructuring effect of the functional (coupling constant: equilibration 10-100 fs with massive and global thermostatting; production 1000 fs with global thermostatting).

Projected NVPT calculations were carried out with the CPMD 4.3[S25–S27] sampling over the previously created FPMD trajectory, using the BLYP functional, the plane wave basis with a cutoff of 100 Ry, Troullier–Martins pseudo potentials[S28] and the Kleinman-Bylander separation scheme.[S29] The trajectory was sampled at every eighth step to form the correlation function, resulting in a time resolution of 4 fs for current and magnetic dipole moments.

The computation of IR and VCD spectra was carried out in the Heisenberg representation using the the Fourier transform of the time-correlation function (FT-TCF) and the newly described gauge for the magnetic dipole moment, as implemented in the python package *ChirPy* 0.21.5, available on GitLab.[S30] See also the provided Jupyter notebook for further details (`https://doi.org/10.5281/zenodo.4776907`).

Adaption of IRSA for Continuous Spectra

We extended the recently presented IRSA algorithm by Riniker and co-workers to continuous spectral densities.[S31] The computational peaks are aligned to their experimental pendants with the Needleman-Wunsch algorithm using a scoring function for peak position and intensity. For the sake of unambiguous alignment we prefer aligning the IR spectra, which is more reliable than seeking for an alignment of the congested VCD spectra. To align with IRSA the spectrum of (1S,2S)-$trans$-1,2-cyclohexanediol, a scoring function was used,[S31]

$$s = \exp\left\{ -\frac{1}{2\sigma_I} \left(\min\left[\frac{I_e}{I_c}, \frac{I_e}{I_c} \right] - \mu_I \right)^2 \right\} \cdot \exp\left\{ -\frac{1}{2\sigma_{\tilde{\nu}}} \left(\frac{\tilde{\nu}_e}{\tilde{\nu}_c} - \mu_{\tilde{\nu}} \right)^2 \right\}, \qquad (23)$$

with standard deviations of $\sigma_I = 0.25$ and $\sigma_{\tilde{\nu}} = 0.025$, expectation values of $\mu_I = 1.0$ and $\mu_{\tilde{\nu}} = 1.0$, and cutoff values of 0.0 a.u. and 40 cm^{-1} for intensities I and wavenumbers $\tilde{\nu}$, respectively. The subscripts e and c stand for experimental and computed values.

To improve the effect of the scoring function, that relies on regions of zeros intensity between peaks, the experimental spectrum was parallel shifted in intensity (Figure S3).
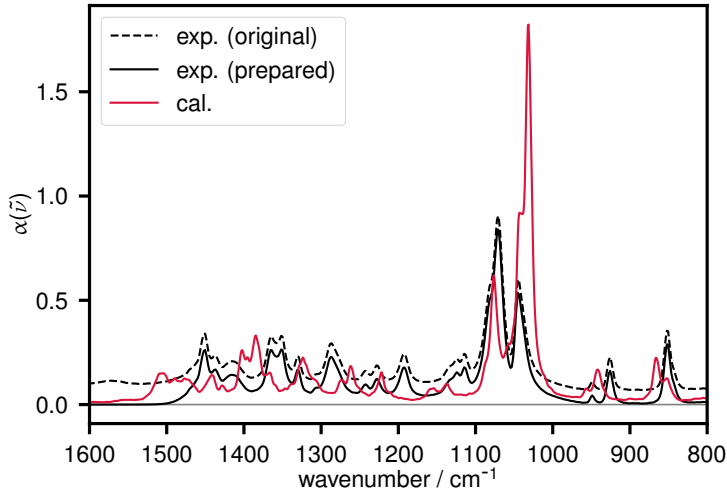

Figure S3: Preparation of the experimental IR spectrum for the application of the IRSA algorithm. Regions of zero intensity are important for the correct calculation of the peak scoring function. The computed spectrum is shown in red.

To preserve peak shapes, parts of the spectrum were protected based on peak intensity,

gradient and second derivative of the computed spectrum. Only "allowed" regions fulfilling $I \leq 80$ M^{-1} cm^{-1} and $dI/d\tilde{\nu} \leq 0.5$ M^{-1} and $d^2I/d\tilde{\nu}^2 \leq 3.12$ M^{-1} cm where eligible for frequency expansion and compression (Figure S4).
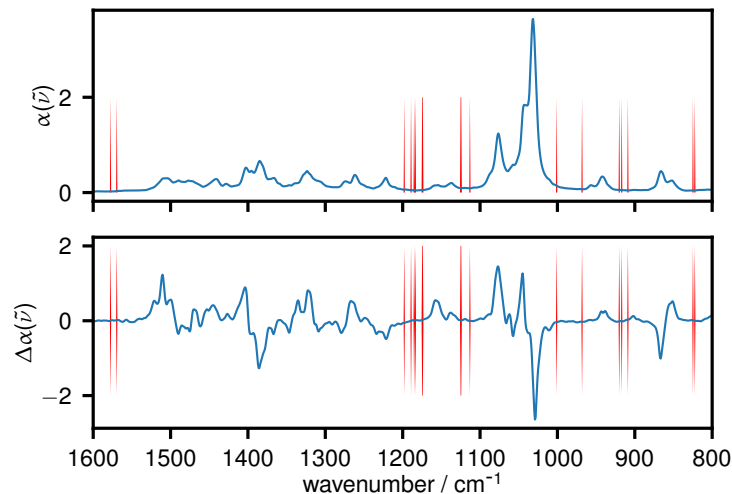

Figure S4: Computed IR an VCD spectra, where red lines mark the zones between peaks that are "allowed" for expansion or compression of the frequency domain.

From the resulting alignment a frequency dependent scaling factor can be calculated, which ranges in the case of (1S,2S)-*trans*-1,2-cyclohexanediol, computed with B3LYP-D3, between 0.975 and 1.01 (Figure S5). The result clearly shows that the functional predicts frequencies with varying accuracy due to the nature of the underlying vibrational mode (bending modes are underestimated, stretching modes are overestimated by the functional).
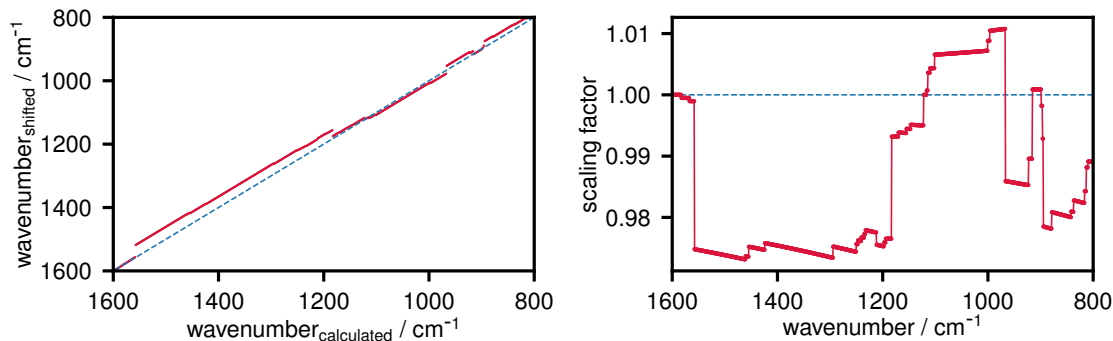

Figure S5: Frequency shift alignment with the IRSA algorithm. Left: Scatter plot of original and shifted frequencies. Right: Resulting frequency-dependent scaling factor.

The new list of frequencies was regularised and the new averaged values for α and $\Delta\alpha$ obtained from cubic interpolation of the old values after relocation to their respective new frequency (with the protected regions defined a priori, the affected values α and $\Delta\alpha$ were always very small though).
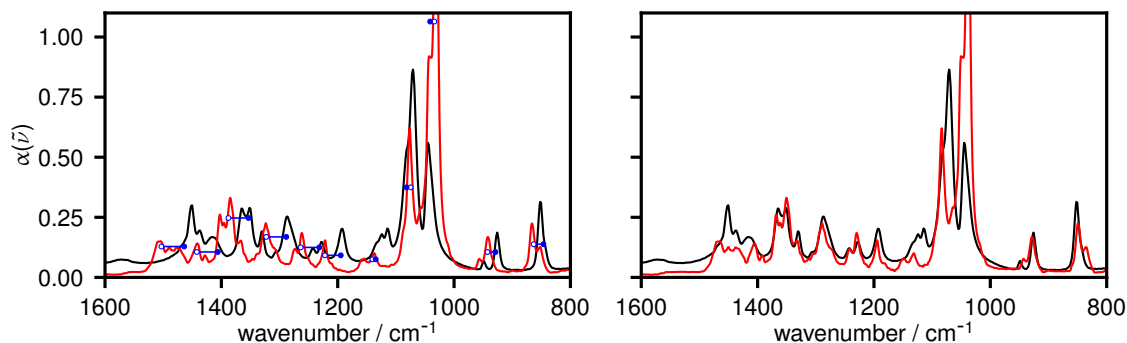

Figure S6: Changed peak position of the calculated spectrum (red) after application of the IRSA algorithm, compared to the experimental spectrum (black).

Other

Plots were generated with python-based Matplotlib 3.0.1.[S32] Molecular visualisations were created with VMD 1.9.3[S33] using the Tachyon Ray Tracer.[S34] All figures were post-processed with Gimp 2.10.18.[S35] Scheme 1 was created with LibreOffice 6.4.7.2[S36]

References

(S1) Marzari, N.; Vanderbilt, D. Maximally Localized Generalized Wannier Functions for Composite Energy Bands. *Phys. Rev. B* **1997**, *56*, 12847–12865.

(S2) Kubo, R.; Toda, M.; Hashitsume, N. In *Statistical Physics II*; Cardona, M., Fulde, P., Queisser, H.-J., Eds.; Springer Series in Solid-State Sciences; Springer Berlin Heidelberg: Berlin, Heidelberg, 1985; Vol. 31.

(S3) Ramírez, R.; López-Ciudad, T.; Kumar P, P.; Marx, D. Quantum Corrections to Classical Time-Correlation Functions: Hydrogen Bonding and Anharmonic Floppy Modes. *The Journal of Chemical Physics* **2004**, *121*, 3973–3983.

(S4) Pérez-Mellor, A.; Barbu-Debus, K. L.; Zehnacker, A. Solid-State Synthesis of Cyclo LD-Diphenylalanine: A Chiral Phase Built from Achiral Subunits. *Chirality* **2020**, *32*, 693–703.

(S5) Li, X.; Porcino, M.; Martineau-Corcos, C.; Guo, T.; Xiong, T.; Zhu, W.; Patriarche, G.; Péchoux, C.; Perronne, B.; Hassan, A.; Kümmerle, R.; Michelet, A.; Zehnacker-Rentien, A.; Zhang, J.; Gref, R. Efficient Incorporation and Protection of Lansoprazole in Cyclodextrin Metal-Organic Frameworks. *International Journal of Pharmaceutics* **2020**, *585*, 119442.

(S6) Pérez-Mellor, A.; Zehnacker, A. Vibrational Circular Dichroism of a 2,5-Diketopiperazine (DKP) Peptide: Evidence for Dimer Formation in Cyclo LL or LD Diphenylalanine in the Solid State. *Chirality* **2017**, *29*, 89–96.

(S7) Sen, A.; Bouchet, A.; Lepère, V.; Le Barbu-Debus, K.; Scuderi, D.; Piuzzi, F.; Zehnacker-Rentien, A. Conformational Analysis of Quinine and Its Pseudo Enantiomer Quinidine: A Combined Jet-Cooled Spectroscopy and Vibrational Circular Dichroism Study. *J. Phys. Chem. A* **2012**, *116*, 8334–8344.

(S8) Merten, C.; Kowalik, T.; Hartwig, A. Vibrational Circular Dichroism Spectroscopy of Solid Polymer Films: Effects of Sample Orientation. *Appl Spectrosc* **2008**, *62*, 901–905.

(S9) Buffeteau, T.; Lagugné-Labarthet, F.; Sourisseau, C. Vibrational Circular Dichroism in General Anisotropic Thin Solid Films: Measurement and Theoretical Approach. *Appl. Spectrosc., AS* **2005**, *59*, 732–745.

(S10) Bebiano, S. V. S.; Rosado, M. T. S.; Castro, R. A. E.; Ramos Silva, M.; Canotilho, J.; Maria, T. M. R.; Eusébio, M. E. S. Polymorphism of Cis-1,4-Cyclohexanediol, a New Plastic Crystal Former. Considerations on Isomeric Cyclohexanediols Plastic Crystal Forming Abilities. *Journal of Molecular Structure* **2014**, *1078*, 10–19.

(S11) The CP2K Developers Group, 2001–2021. `https://www.cp2k.org`.

(S12) Case, D. A.; Aktulga, H. M.; Belfon, K.; Ben-Shalom, I. Y.and Brozell, S. R.; Cerutti, D. S.; Cheatham, T. E.; Cruzeiro, V. W. D.; Darden, T. A.; Duke, R. E.; Giambasu, G.; Gilson, M. K.; Gohlke, H.; Goetz, A. W.; Harris, R.; Izadi, S.; Izmailov, S. A.; Jin, C.; Kasavajhala, K.; Kaymak, M. C.; King, E.; Kovalenko, A.; Kurtzman, T.; Lee, T. S.; LeGrand, S.; Li, P.; Lin, C.; Liu, J.; Luchko, T.; Luo, R.; Machado, M.; Man, V.; Manathunga, M.; Merz, K. M.; Miao, Y.; Mikhailovskii, O.; Monard, G.; Nguyen, H.; O'Hearn, K. A.; Onufriev, A.; Pan, F.; Pantano, S.; Qi, R.; Rahnamoun, A.; Roe, D. R.; Roitberg, A.; Sagui, C.; Schott-Verdugo, S.and Shen, J.; Simmerling, C. L.; Skrynnikov, N. R.; Smith, J.; Swails, J.; Walker, R. C.; Wang, J.; Wei, H.; Wolf, R. M.; Wu, X.; Xue, Y.; York, D. M.; Zhao, S.; Kollman, P. A. Amber20. University of California, San Francisco, 2020; `www.ambermd.org`.

(S13) VandeVondele, J.; Krack, M.; Mohamed, F.; Parrinello, M.; Chassaing, T.; Hutter, J. QUICKSTEP: Fast and Accurate Density Functional Calculations Using a Mixed Gaussian and Plane Waves Approach. *Comput. Phys. Commun.* **2005**, *167*, 103–128.

(S14) Stephens, P. J.; Devlin, F. J.; Chabalowski, C. F.; Frisch, M. J. Ab Initio Calculation of Vibrational Absorption and Circular Dichroism Spectra Using Density Functional Force Fields. *J. Phys. Chem.* **1994**, *98*, 11623–11627.

(S15) Becke, A. D. Density-functional Thermochemistry. III. The Role of Exact Exchange. *The Journal of Chemical Physics* **1993**, *98*, 5648–5652.

(S16) Becke, A. D. Density-Functional Exchange-Energy Approximation with Correct Asymptotic Behavior. *Phys. Rev. A* **1988**, *38*, 3098–3100.

(S17) Lee, C.; Yang, W.; Parr, R. G. Development of the Colle-Salvetti Correlation-Energy Formula into a Functional of the Electron Density. *Phys. Rev. B* **1988**, *37*, 785–789.

(S18) Vosko, S. H.; Wilk, L.; Nusair, M. Accurate Spin-Dependent Electron Liquid Correlation Energies for Local Spin Density Calculations: A Critical Analysis. *Can. J. Phys.* **1980**, *58*, 1200–1211.

(S19) VandeVondele, J.; Hutter, J. Gaussian Basis Sets for Accurate Calculations on Molecular Systems in Gas and Condensed Phases. *J. Chem. Phys.* **2007**, *127*, 114105.

(S20) Goedecker, S.; Teter, M.; Hutter, J. Separable Dual-Space Gaussian Pseudopotentials. *Phys. Rev. B* **1996**, *54*, 1703–1710.

(S21) Hartwigsen, C.; Goedecker, S.; Hutter, J. Relativistic Separable Dual-Space Gaussian Pseudopotentials from H to Rn. *Phys. Rev. B* **1998**, *58*, 3641–3662.

(S22) Krack, M. Pseudopotentials for H to Kr Optimized for Gradient-Corrected Exchange-Correlation Functionals. *Theor. Chem. Acc.* **2005**, *114*, 145–152.

(S23) Grimme, S.; Antony, J.; Ehrlich, S.; Krieg, H. A Consistent and Accurate Ab Initio Parametrization of Density Functional Dispersion Correction (DFT-D) for the 94 Elements H-Pu. *J. Chem. Phys.* **2010**, *132*, 154104.

(S24) Bussi, G.; Donadio, D.; Parrinello, M. Canonical Sampling through Velocity Rescaling. *J. Chem. Phys.* **2007**, *126*, 014101.

(S25) Scherrer, A.; Vuilleumier, R.; Sebastiani, D. Nuclear Velocity Perturbation Theory of Vibrational Circular Dichroism. *J. Chem. Theory Comput.* **2013**, *9*, 5305–5312.

(S26) Scherrer, A.; Vuilleumier, R.; Sebastiani, D. Vibrational Circular Dichroism from Ab Initio Molecular Dynamics and Nuclear Velocity Perturbation Theory in the Liquid Phase. *J. Chem. Phys.* **2016**, *145*, 084101.

(S27) CPMD 4.1.0, Copyright 2000–2019. IBM Corp. and by Max Planck Institute, Stuttgart, `https://www.cpmd.org`.

(S28) Troullier, N.; Martins, J. L. Efficient Pseudopotentials for Plane-Wave Calculations. *Phys. Rev. B* **1991**, *43*, 1993–2006.

(S29) Kleinman, L.; Bylander, D. M. Efficacious Form for Model Pseudopotentials. *Phys. Rev. Lett.* **1982**, *48*, 1425–1428.

(S30) Jähnigen, S. ChirPy – A Python Package for Analysing Supramolecular and Electronic Structure, Chirality and Dynamics (Version 0.21.5). Zenodo, 2021; `http://doi.org/10.5281/zenodo.4775330`.

(S31) Böselt, L.; Dötzer, R.; Steiner, S.; Stritzinger, M.; Salzmann, S.; Riniker, S. Determining the Regiochemistry and Relative Stereochemistry of Small and Druglike Molecules Using an Alignment Algorithm for Infrared Spectra. *Anal. Chem.* **2020**, *92*, 9124–9131.

(S32) Hunter, J. D. Matplotlib: A 2D Graphics Environment. *Comput. Sci. Eng.* **2007**, *9*, 90–95.

(S33) Humphrey, W.; Dalke, A.; Schulten, K. VMD – Visual Molecular Dynamics. *J Mol Graph* **1996**, *14*, 33–38.

(S34) Stone, J. Tachyon. An Efficient Library for Parallel Ray Tracing and Animation. 1995; `jedi.ks.uiuc.edu/~johns/raytracer`.

(S35) GIMP 2.8. `gimp.org`.

(S36) The LibreOffice Contributors, 2000–2020. `www.libreoffice.org`.